Journal of Loss Prevention in the Process Industries 99 (2026) 105822

Contents lists available at ScienceDirect

Journal of Loss Prevention in the Process Industries

journal homepage: www.elsevier.com/locate/jlp

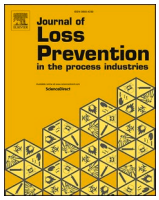

Influence of active mitigation barriers with fans on dense gas dispersion

Alessandro Pinciroli, Renato Rota, Valentina Busini *

Politecnico di Milano, Department of Chemistry, Materials and Chemical Engineering "Giulio Natta", Italy

ARTICLE INFO

Keywords:
Active mitigation barriers
Heavy gas dispersion
Liquefied natural gas (LNG)
Safety

ABSTRACT

The situation in the global energy market has recently led to a sharp increase in the number of regasification terminals to import natural gas in liquefied form (LNG). Because of the hazard of these systems and the risk of fire and explosion due to possible accidental breakages, in recent years the technical community has been trying to define solutions for the mitigation of the consequences of major accidents. In previous works, methodologies for the design of containment wall of possible explosive cloud and curtains of vapor/air have been defined. The aim of this study is the suggestion of an active barrier and the definition of a methodology that allows to determine the airflow rate, generated by fans, required to dilute an LNG flammable cloud down to LFL. Results showed that with the proposed methodology the designed active barrier is able to stop the cloud at its location, minimizing the consequences of the release and improving the performance of a passive barrier.

1. Introduction

The situation in the global energy market has recently led to a sharp increase in the number of proposals for the construction of regasification terminals to import liquefied natural gas (LNG). The increasing use of LNG is driven by its advantages as a cleaner alternative to traditional fossil fuels, particularly in the context of global energy transition and environmental sustainability. LNG lower carbon emissions compared to coal and oil make it a favourable option for reducing greenhouse gas emissions in various sectors, including transportation and power generation (Ayorinde et al., 2024; Daudu et al., 2024; Lim et al., 2013). The safety of LNG regasification plants is a critical concern due to the inherent risks associated. The regasification process involves several stages, including the transfer of LNG from carriers to storage tanks, and subsequently to regasification units and to distribution networks (Naveiro et al., 2021; Shingan et al., 2024). The gas-air mixture arising from an accidental release of LNG and its vaporization and dispersion is flammable in a concentration range between 4.4 % (LFL) and 15 % (UFL) in volume (Baalisampang et al., 2019; Sun et al., 2015; Yun et al., 2011).

When LNG leaks, it can form a boiling pool on the ground at a very low temperature, resulting in very cold and dense vapours above the pool, which can create a hazardous environment (Nerheim et al., 2021); this makes gas cloud generated from LNG evaporation double interesting because it is also representative of dense gas clouds. In this study, several accidental scenarios involving the rupture of pipes carrying LNG at −162 °C, were analysed, with particular reference to the evaporation of the LNG pool leading to a flammable cloud. During the dispersion phase, flammable vapours mix with the environmental air creating a gas/air mixture heavier than air. When a cloud is heavier than air two effects can be observed: the reduction of vertical mixing due to atmospheric turbulence and the lateral spread of the cloud. These effects are due to the stratification of the dense gas and therefore to the density gradients that are formed. The combination of these two effects leads to a cloud lower and wider than the one observed in case of neutral gas release (Koopman and Ermak, 2007; Wingstedt et al., 2017).

There are several ways to mitigate the hazards related to flammable clouds of dense gas (Diaz-Ovalle et al., 2012; Kim et al., 2014); in previous studies, the mitigation through passive barriers has been studied (Bellegoni et al., 2021; Busini et al., 2012; Derudi et al., 2014; Lim et al., 2017; Lyu et al., 2018), as well as the use of active barriers with curtains of water vapor/air (Brown et al., 1990; Buchlin, 2017; Diaz-Ovalle et al., 2012; Fthenakis and Blewitt, 1993; Kim et al., 2012; Marsegan et al., 2016; Min et al., 2020; Olewski et al., 2011; Qi et al., 2016; Rana et al., 2010; Rana and Mannan, 2010). Because one of the main characteristics of cold dense clouds is their tendency to reduce turbulence (Koopman et al., 1989), the active barriers base their efficacy on the capability to increase it. A recent study has shown the higher efficacy of an active barrier equipped with fans (i.e., a barrier releasing airflow generated by fans embedded in the mitigation barriers) compared to a passive one (Pinciroli et al., 2024). What is lacking is a criterion for the design of such a mitigation measure; to develop such a criterion is the main aim of

* Corresponding author.
E-mail address: valentina.busini@polimi.it (V. Busini).

https://doi.org/10.1016/j.jlp.2025.105822
Received 7 March 2025; Received in revised form 22 August 2025; Accepted 22 October 2025
Available online 22 October 2025

Table 1
Geometric parameters of the domain.

	Case study A	Case study B
Lenght (axis z)	400 m	800 m
Width (axis x)	300 m	800m
Height (axis y)	30 m	45 m
Pool diameter	20 m	20 m
Pool distance from the origin	220 m	200 m
Distance of the wall from the pool	50 m	150 m
Barrier height (axis z)	2.5 m	6 m
Barrier width (axis y)	310 m	700 m
Barrier thickness (axis x)	0.5 m	0.5 m

Table 2
Boundary conditions.

Ground	Wall @ 298 K, roughness = 0.01 m
Barrier	Adiabatic wall, roughness = 0.01 m
Pool	During atmospheric stabilization: Wall @ 298 K, roughness = 0.01 m During pool evaporation: Mass flow inlet
Fans	Interior/Fan
Wind inlet, domain sides, sky	Velocity inlet
Wind outlet	Pressure outlet

this work.

When designing any active barrier system, the key factor is determining the required flow rate of the diluent—be it air, water, or steam—to inject into the dense gas cloud to reduce its concentration to the target level. Following the approach of Diaz-Ovalle et al. (2012), and more specifically Marsegan et al. (2016) and (Pinciroli et al., 2024), this work proposes a methodology to size the fan-activated barriers proposed in Pinciroli et al. (2024) to dilute the cloud of LNG below the lower flammability limit (LFL) before the cloud overcomes the barrier. The choice of such a concentration is linked to the flash fire scenario, which is a reasonable scenario expected in the case of late ignition of a cloud of flammable material. If the LFL concentration boundary (which is a reasonable fatality threshold estimation in case of flash-fire) is contained inside the plant, the societal risk would be reduced correspondingly.

This study investigates two case studies: a discharge through a 50 mm orifice on a pipeline with a diameter of 1 m, representative of a major accident realistic scenario in the frame of a QRA, and a catastrophic release resulting from a full-bore rupture of the same pipeline, representative of the worst case catastrophic scenario. Computational fluid dynamics (CFD), a technique that has been largely used and validated for modelling dense gas cloud spills in the last years through various works (Bellegoni et al., 2022; Gavelli et al., 2008; S. M. Tauseef et al., 2011; Seshu et al., 2005), was used to predict the hazardous distance for various accidental scenarios.

The paper is organized as follow.

- in section 2 the CFD settings and the proposed methodology for the design of the active barrier are provided;
- in section 3 and 4 the former and latter case studies and the results obtained by sizing the number of fans through the proposed methodology are presented;
- in section 5 the main conclusions are deduced.

2. Materials and methods

Geometries and mesh required by the CFD approach were created with the software ANSYS Spaceclaim® and ANSYS Fluent meshing® (ANSYS Inc, 2023a) respectively; the main characteristics of the computational domain are reported in Tables 1 and 2; the mesh consists of about 3–5 milions elements depending on the case studied with the following sizing: on the fan boundaries the maximum size of is 0.08 m, while for the pool source a mesh of 0.1 m was used. On the ground the mesh size is 0.9 m and a proximity parameter of 10 cells per gaps was added on the overall surface mesh with a maximum cell length of 3.2 m. The growth rate is 1.1 on all the surfaces except for the barrier and fans where a factor of 1.05 was used. Ten inflation layers were added on solid surfaces and finally a poly-hexcore volume mesh was generated with a lower cell orthogonal quality of 0.2. A symmetry plane was not necessary since the domain was simulated entirely. The mesh independence analysis is reported in the Supplementary material. Moreover, with respect to the fans, the embedded boundary condition was used, by describing the prevalence of the fan through the polynomial equation reported in the Supplementary Material (ANSYS Inc, 2023b).

Table 3
Solver settings.

Solution Method	Scheme
Pressure-velocity coupling	PISO
Spatial discretization	Scheme
Gradient	Least square cell based
Pressure	PRESTO!
Density	Second order upwind
Momentum	Second order upwind
Turbulent kinetic energy	Second order upwind
Energy	Second order upwind
Specific dissipation rate	Second order upwind
Other settings	
Gravity	-9.81 m/s^2 along y-direction
Iterations	Until convergence criteria are reached
Initialisation scheme	Hybrid
Convergence Criteria	
Continuity	0.003
X – velocity	0.001
Y – velocity	0.001
Z – velocity	0.001
Energy	1e-6
K	0.001
omega	0.001
CH_4	0.004

The commercial package Ansys Fluent® 23 (ANSYS Inc, 2023b) was used for all the computations with the double precision solver. The k–ω SST model was chosen to reproduce the effect of the turbulence in the domain, (Busini et al., 2012; Busini and Rota, 2014; Derudi et al., 2014; Eberwein et al., 2020; Marsegan et al., 2016).

The domain boundary conditions are reported in Table 2; for the velocity inlets, a power law wind profile considering a 5D Pasquill stability class (i.e., velocity 5 m/s at 10 m height and neutral stability) was chosen to model atmospheric conditions as it is considered a "typical" day (Ennis, 2006). The profile was implemented through a power law:

$$u_w(y) = u_{w10} \times \left(\frac{y}{10}\right)^{\beta} \quad (1)$$

Where.

- u_{w10} is the wind velocity at 10 m above ground
- y is the height above ground
- $\beta = 0.25$ is a factor that consider atmospheric stability and ground type (Crowl and Louvar, 2019)

Solver settings and convergence criteria are reported in Table 3 following the options suggested in the software manual (ANSYS Inc, 2023b) for transient simulations.

2.1. Proposed methodology for sizing the active barrier

Following the same procedures discussed elsewhere (Derudi et al., 2014; Marsegan et al., 2016), the simulation of open-field cloud dispersion, in which the release takes place without any mitigation wall, was preliminary performed for the definition of the minimum size (H_{obs}

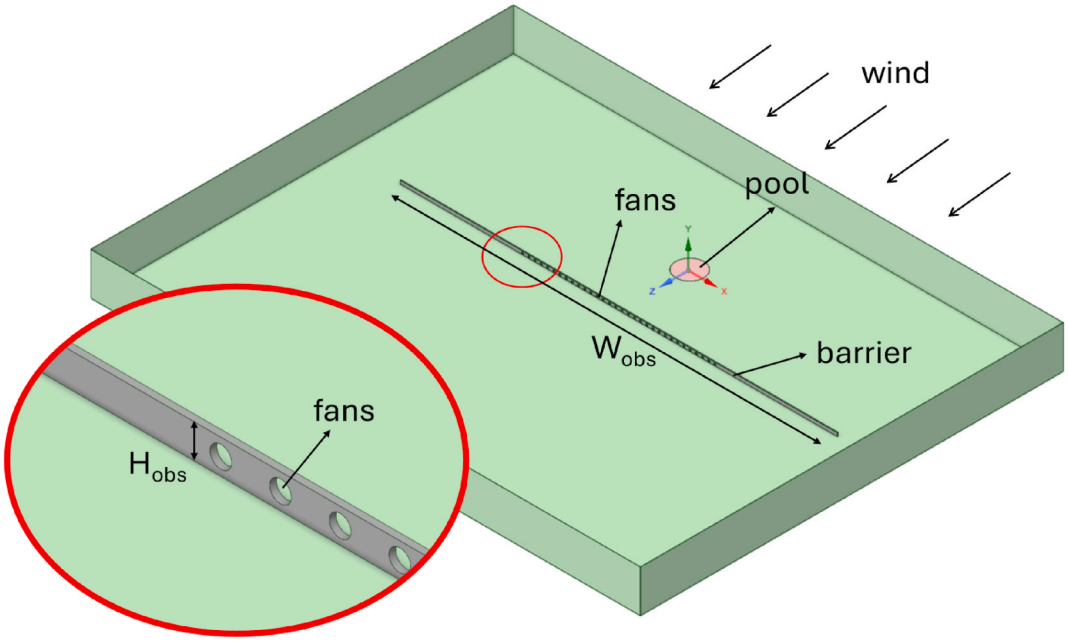

Fig. 1. Integration domain.

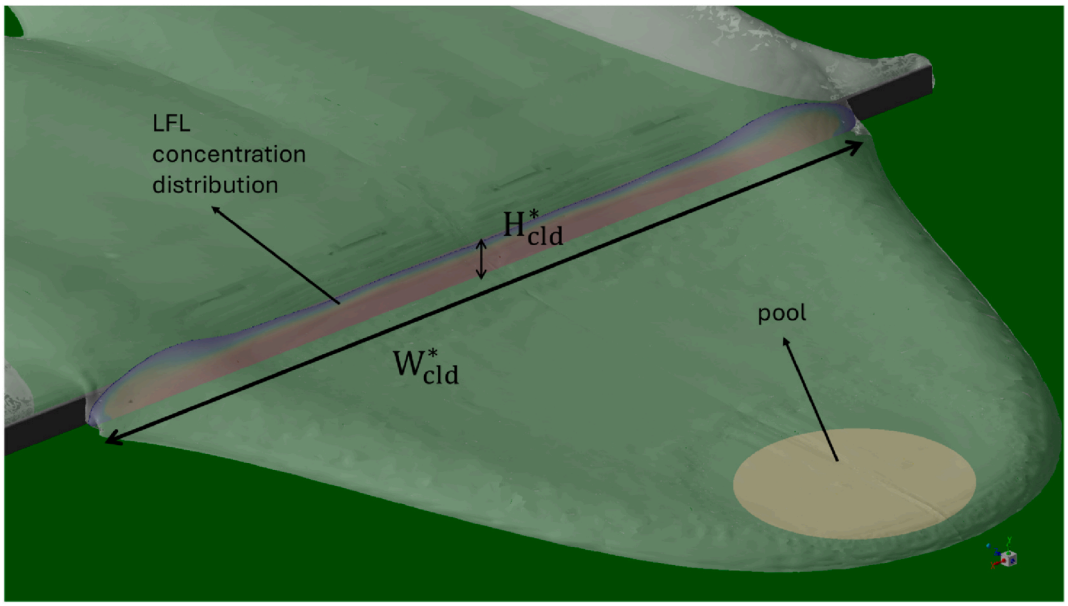

Fig. 2. Characteristic cloud parameters in the presence of the passive barrier.

and W_{obs} see Fig. 1) of the mitigation barrier able to influence cloud dispersion, according to the procedure discussed in detail elsewhere (Busini et al., 2012; Derudi et al., 2014).

Such a procedure is based on the definition of a dimensionless parameter, which is the ratio between the height of the barrier, H_{obs} (or the barrier width W_{obs}), and the cloud height H_{cld} (or the cloud width W_{cld}) evaluated in open field conditions at the same distance from the source:

$$R^* = \min\left(\frac{H_{obs}}{H_{cld}}, \frac{W_{obs}}{W_{cld}}\right) \tag{2}$$

For values of $R^* \geq 1$ the obstacles influence the cloud dispersion, or even block it (Derudi et al., 2014).

The second step is the simulation of cloud dispersion in the presence of a passive mitigation barrier (e.g., a wall) with $R^* = 1$. With this simulation it is possible to compute the cloud width (W^*_{cld}) and height (H^*_{cld}), and its maximum concentration (C_{max}), in correspondence of the barrier position (see Fig. 2)

Being Q_c the flammable cloud flow rate [m^3/s] estimated at the barrier, C_c the average flammable gas concentration at the same position [mol/mol] and Q_a the air flow rate [m^3/s] forced into the cloud by the active barrier fans, reducing the concentration of the cloud at the barrier below the lower flammability limit (LFL [mol/mol]), requires:

$$\frac{Q_c \cdot C_c}{Q_{tot}} = \frac{Q_c \cdot C_c}{Q_c + Q_a} = LFL \tag{3}$$

Defining $\alpha = \frac{C_c}{LFL}$,the previous equation can be recast in:

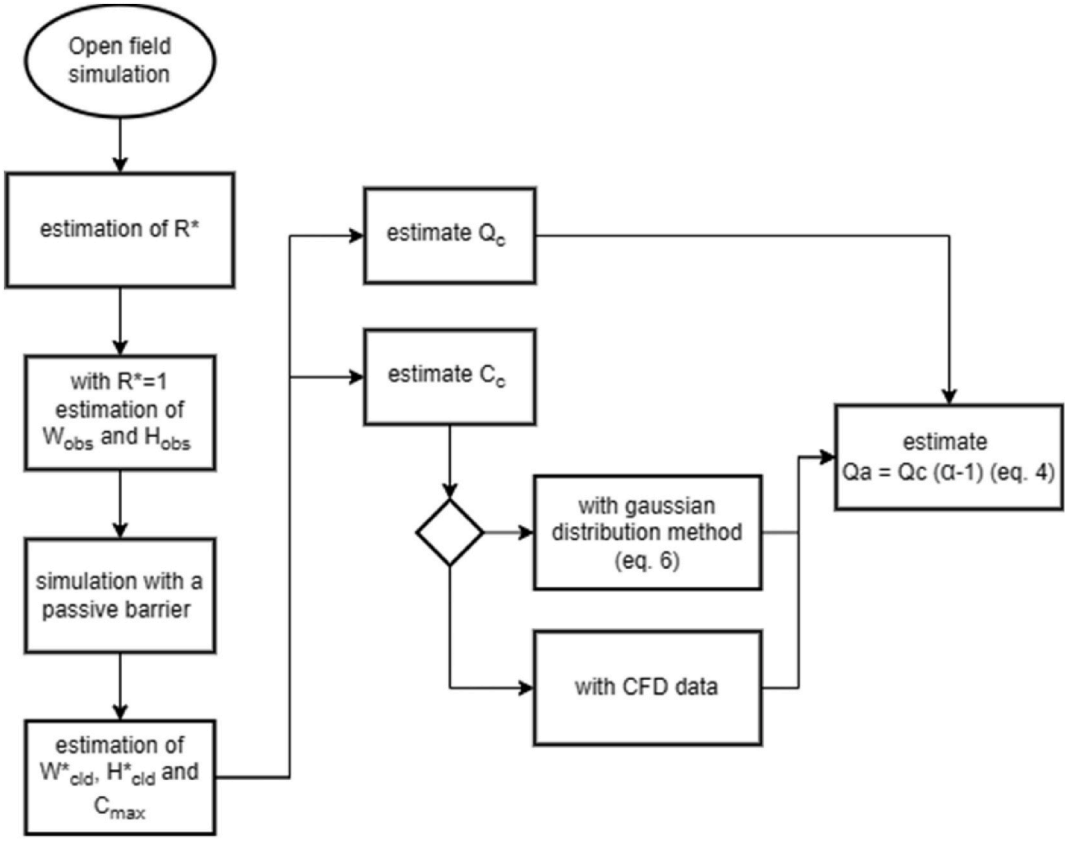

Fig. 3. Flowchart of the main steps to calculate the ideal flow rate to dilute the cloud.

$$Q_a = Q_{tot} - Q_c = Q_c \cdot (\alpha - 1) \tag{4}$$

Q_c can be estimated through characteristics cloud parameters computed through the CFD simulation in the presence of the passive barrier ($H^*_{cld} \cdot W^*_{cld}$), and to the mean cloud velocity computed during the simulation with only the passive mitigation barrier through the following relation:

$$Q_c = H^*_{cld} \cdot W^*_{cld} \cdot u_{cld} \tag{5}$$

Assuming that the concentration distribution along the y dimension is gaussian, it is possible to estimate C_C as (Marsegan et al., 2016):

$$\int_{-\frac{W^*_{cld}}{2}}^{+\frac{W^*_{cld}}{2}} \frac{const}{\sigma_y \sqrt{2\pi}} \exp\left(-\frac{\left(W^*_{cld}\right)^2}{2\sigma_y^2} \right) dy = 2\, C_C\, W^*_{cld} \tag{6}$$

Where.

- The boundary condition $C(y=0) = \frac{const}{\sigma_y \sqrt{2\pi}} = C_{max}$ is used to obtain the value of the constant; C_{max} is the maximum concentration in the

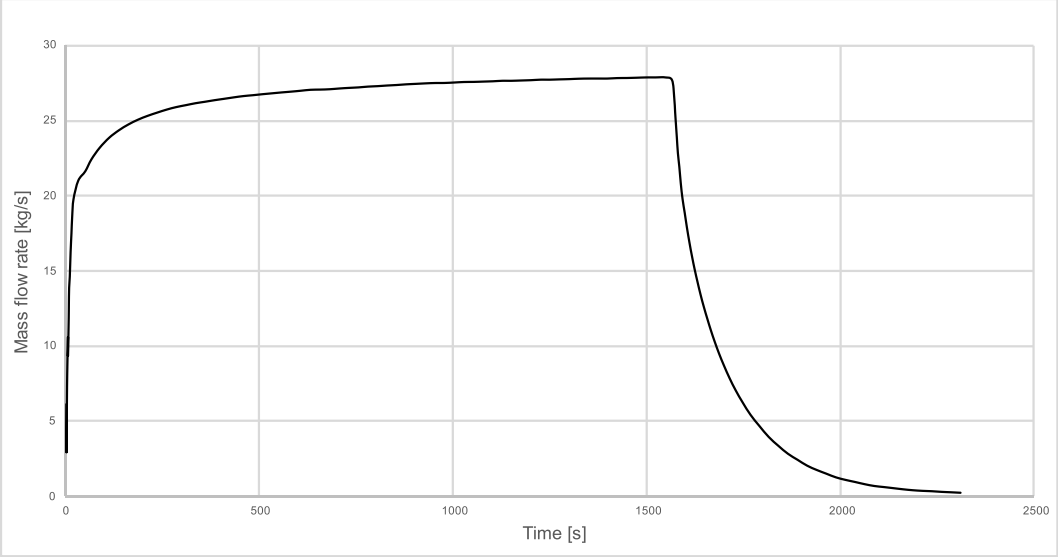

Fig. 4. Pool evaporation rate for case A.

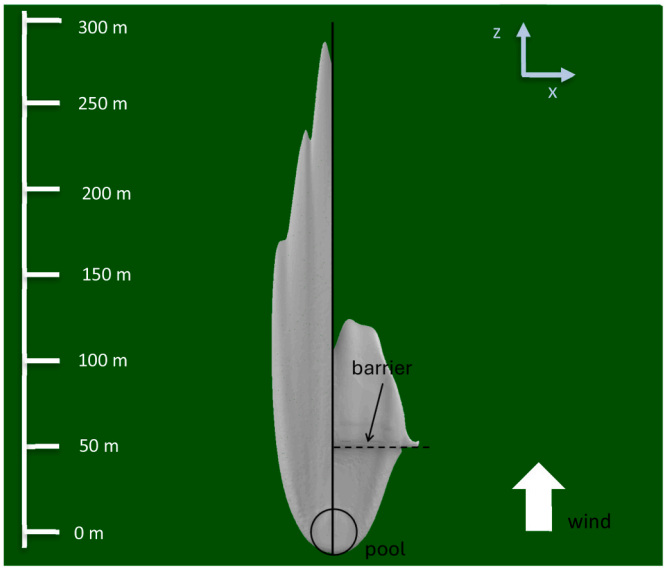

Fig. 5. LFL cloud envelope in open field (left) and with the passive barrier (right).

cloud when it reaches the wall position and is taken from the open field CFD simulation.

- $-\frac{W^*_{cld}}{2}$ and $+\frac{W^*_{cld}}{2}$ are the coordinates of the maximum and minimum lateral span of the LFL cloud (i.e., half of the cloud width)
- σ_y is the y dispersion parameter and is computed by forcing the gaussian concentration distribution at $y = \frac{W^*_{cld}}{2}$ to be equal to LFL, resulting in $\sigma_y \approx \frac{W^*_{cld}}{\sqrt{2 \ln \frac{C_{max}}{LFL}}}$;

In Fig. 3 a flowchart shows the main steps of the procedure proposed to estimate the theoretical air flow rate to be provided by the active barrier.

The mean flammable concentration calculated using Eq. (6) can also be obtained directly from the CFD simulation, as is done for the maximum concentration. Both results are consistent, with the simulation data showing a value of molar fraction 12 % lower (0.19) than that obtained through the Gaussian approach (0.21). Since the aim of the work is to provide a safety device able to reduce the extension of dense gas clouds, it was chosen to use the higher mean concentration value resulting in a conservative approach.

3. Case study A

The first case study concerns an accidental scenario involving a leak from a 50 mm hole on a pipeline 1 m in diameter, which carries LNG at −161.4 °C. The hole diameter was chosen considering that small leaks due to corrosion or manufacturing defects are realistically more frequent than full bore ruptures (Casal, 2008; Uijt de Haag et al., 2001). As made in previous studies (Busini and Rota, 2014; Marsegan et al., 2016), the source term, estimated using PHAST 9.1 (PHAST, 2024) was simulated in the CFD code through an UDF (User Defined Function) that defines the time – dependent mass flow rate from a pool of constant radius of 20 m, as shown in Fig. 4 and reported in the Supplementary Materials. A second UDF was implemented to extract from the simulation results the maximum hazardous area in terms of concentration values larger than LFL in the domain during the release (see the Supplementary Materials for the script).

3.1. Open field and passive barrier scenario

Before the release of methane (which was used in all the simulations as a proxy of LNG), a simulation was performed to stabilize atmospheric conditions and develop a wind profile across the domain. Afterward, the mass flow from the pool was set using the time-dependent profile of Fig. 4 to obtain the cloud dimensions in open field (i.e., without any mitigation barrier). From the results of the open field simulation the parameters required to size the passive mitigation barrier were computed as previously discussed. The flammable cloud reached a maximum length of about 290 m from the pool centre and a maximum width of about 74 m, while the mean height of the cloud was about 2.5 m. The barrier was sized to cover entirely the cloud at an arbitrary distance of 50 m downwind from the pool, which is compatible with a realistic case of a perimetral wall of a plant, that is: $H_{obs} = H_{cld} = 2.5$ m and $W_{obs} = 100$ m $> W_{cld} = 74$ m.

The passive barrier simulation showed that the barrier reduces the cloud maximum length to 125 m from the boiling pool centre as shown in Fig. 5 (i.e., 57 % less than the open field case) and was used to estimate, as discussed previously the parameters summarized in Table 4 for the design of the active barrier together with equations (3)–(6).

Table 4
Active barrier parameters computed using the proposed procedure for case study A.

H^*_{cloud}	3.25 m
W^*_{cloud}	82 m
C_{max}	37 %
Q_c	338.5 m^3/s
C_c	21 %
α	4.88
Q_a	1314 m^3/s

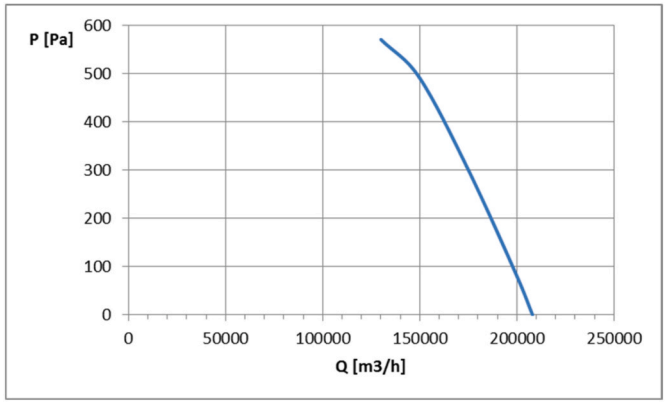

Fig. 6. Fan performance curve (DYNAIR, 2025).

3.2. Active barrier scenarios

3.2.1. Active barrier with 32 fans – reference configuration

The axial fans to be embedded in the wall were chosen with a diameter of 1.6 m, a yield of 60 % and a required power of 55 kW resulting in about 32 fans to be embedded in the wall to provide the estimated Q_a flow rate. Fig. 6 shows the characteristic curve of the fans selected among the several available on the market (other information and fan-layout scheme can be found at (DYNAIR, 2025) while the polynomial equation used for imputing the performance curve of the fan in the embedded boundary condition in ANSYS Fluent (ANSYS Inc, 2023b) can be found in Fig. S2 of the Supplementary Material.

$$N^{\circ}_{fan} = \frac{Q_a}{Q_{fan}} = 32 \tag{7}$$

Preliminary simulations showed that the cloud overcomes the wall by the sides due to the recirculation of air induced by fans just before the barrier. Therefore, it was decided to increase the width of the barrier by

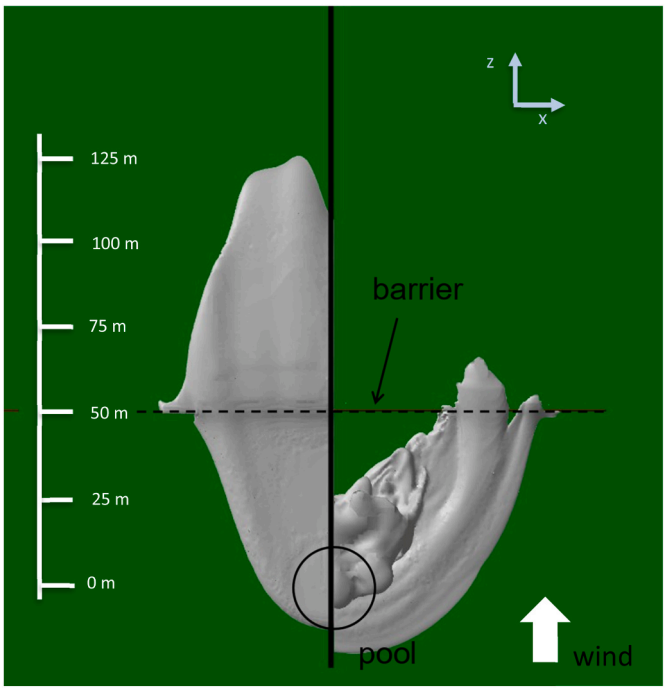

Fig. 7. LFL cloud envelope with the passive barrier (left) and with the 32 fans on 82 m active barrier (right).

about three times to 310 m to avoid the problem. Fans were placed on a single row centred at half the height with a spacing between their axes of 2.54 m, to cover the entire width W_{cld} of 82 m. Fig. 7 shows the simulation results; we can see that the maximum downwind distance reached by the cloud from the boiling pool is about 67 m, that is 77 % less when compared to the open field simulation and 46 % less when compared to the passive barrier case. Therefore, a first downside of using active barrier equipped with fans seems to be a large increase of the barrier size.

In fact, as previously mentioned, the lateral spread of the flammable cloud is greater than the one in the passive barrier scenario. Thus, the cloud overcomes the active barrier where no embedded fans are present. As a reference, this scenario will be compared to other configurations of the active barrier design to investigate the effect of changing some design parameters.

3.2.2. *Active barrier with 32 fans – second configuration*

To avoid the cloud overcoming the barrier where the fans are not present, a second simulation was carried out with a different placement of the active devices. Starting from the reference configuration with 32 fans, the total width of the cloud (148 m) was used to size the new configuration, where the total span of the devices is 140 m.

As excepted, the results of the simulation showed the same phenomenon as in the reference configuration, with the cloud expanding laterally even more, up to about 210 m. As shown in Fig. 8, the central part of the cloud is still unable to reach and overcome the barrier, leading the cloud to reach about 69 m from the pool centre like the reference case. The main input of the simulation are summarized in Table 5 while the main results are reported in Table 5 and Fig. 12.

3.2.3. *Active barrier with 32 fans – third configuration*

Further increasing the length of the barrier where the 32 fans are installed up to 200 m was able to stop the cloud at the barrier while avoiding it to overcome the barrier laterally due to recirculation, as shown in Fig. 9.

The main input of the simulation are summarized in Table 5 while the main results are reported in Table 5 and Fig. 12.

For this specific case, which is highly representative of Case A, the Supplementary Material includes a time-lapse image (Fig. S3) and a video showing the evolution of the cloud contour at the LFL concentration threshold over time. This visualization provides valuable insights from an emergency-response planning perspective, as it illustrates how the hazardous area develops and changes during the event. Moreover, a couple of examples of the vector fields are provided (Fig. S4).

3.2.4. *Active barrier with 25 fans*

To compare the effect of the number of fans with respect to the length of the active barrier, a new configuration of the active barrier involving 25 fans embedded in 200 m of barrier was investigated. The total air flow rate in this configuration is 1028 $\frac{m^3}{s}$ which is 22 % lower than the theoretical one. As shown in Fig. 10, in this case the cloud overcomes the barrier in the central zone but not at the edges of the barrier, thanks to

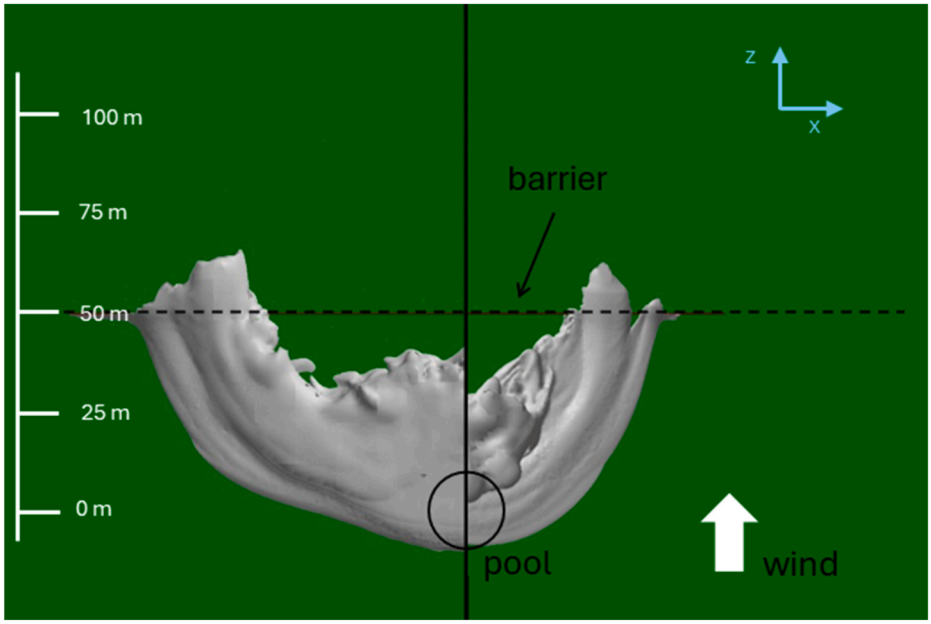

Fig. 8. LFL cloud envelope with the 32 fans on 140 m (left) and in the reference configuration (right).

Table 5
Input of the simulations in terms of number of fans, width of wall along which they are distributed and volumetric flow rate of air obtained and output in terms of percentage difference of the cloud dimension at the LFL concentration with respect to the open field scenario for the various barrier configurations.

		run	Number of fans	Power demand [MW]	Barrier width [m]	Barrier width with fans embedded [m]	Qa [m3/s]	Length change [%]	Width change [%]	Height change [%]
Wind speed 5 m/s @10m	Passive barrier	2	0	0	200	–	0	−57	+11	+32
	Active barrier	3	32	1.8	310	82	1314	−77	+100	+171
		4	32	1.8	310	140	1314	−76	+184	+219
		5	32	1.8	310	200	1314	−81	+200	+447
		6	25	1.4	310	200	1028	−74	+173	+469
		7	19	1	310	132	780	−72	+116	+550

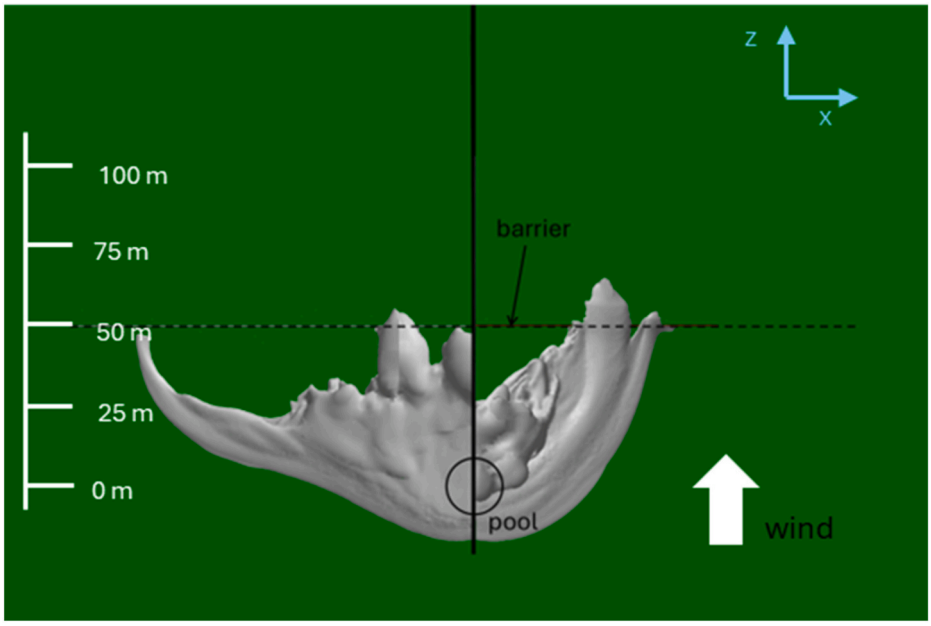

Fig. 9. LFL cloud envelope with the 32 fans on 200 m (left) and in reference configuration (right).

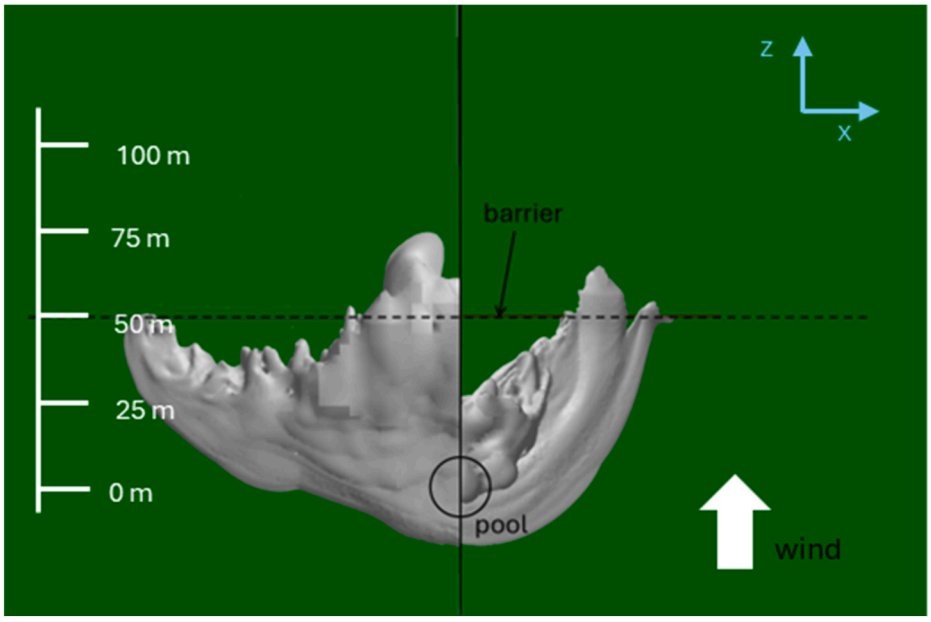

Fig. 10. LFL cloud envelope with the 25 fans on 200 m (left) and in the reference configuration (right).

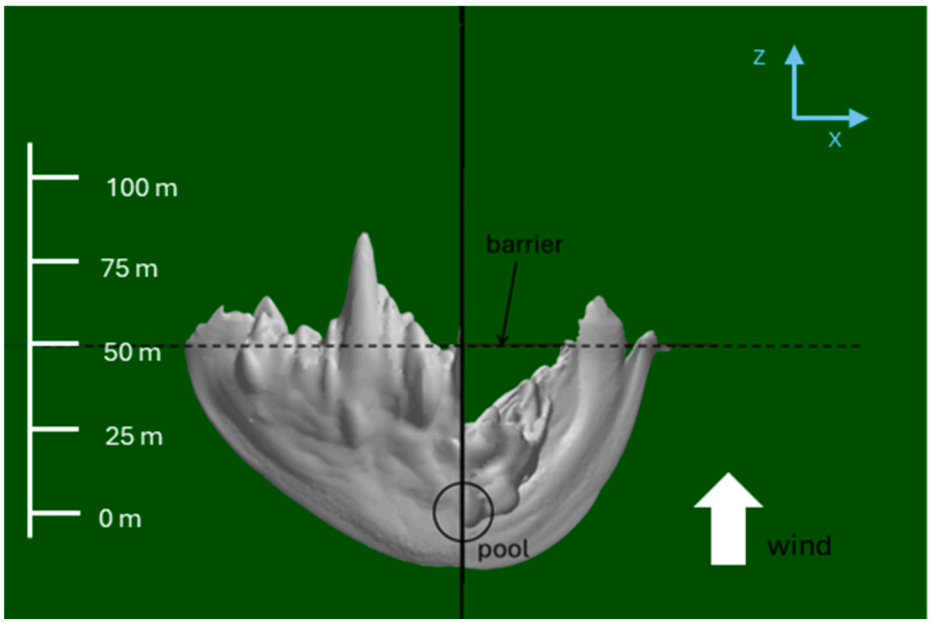

Fig. 11. LFL cloud envelope with the 19 fans (left) and in the reference configuration (right).

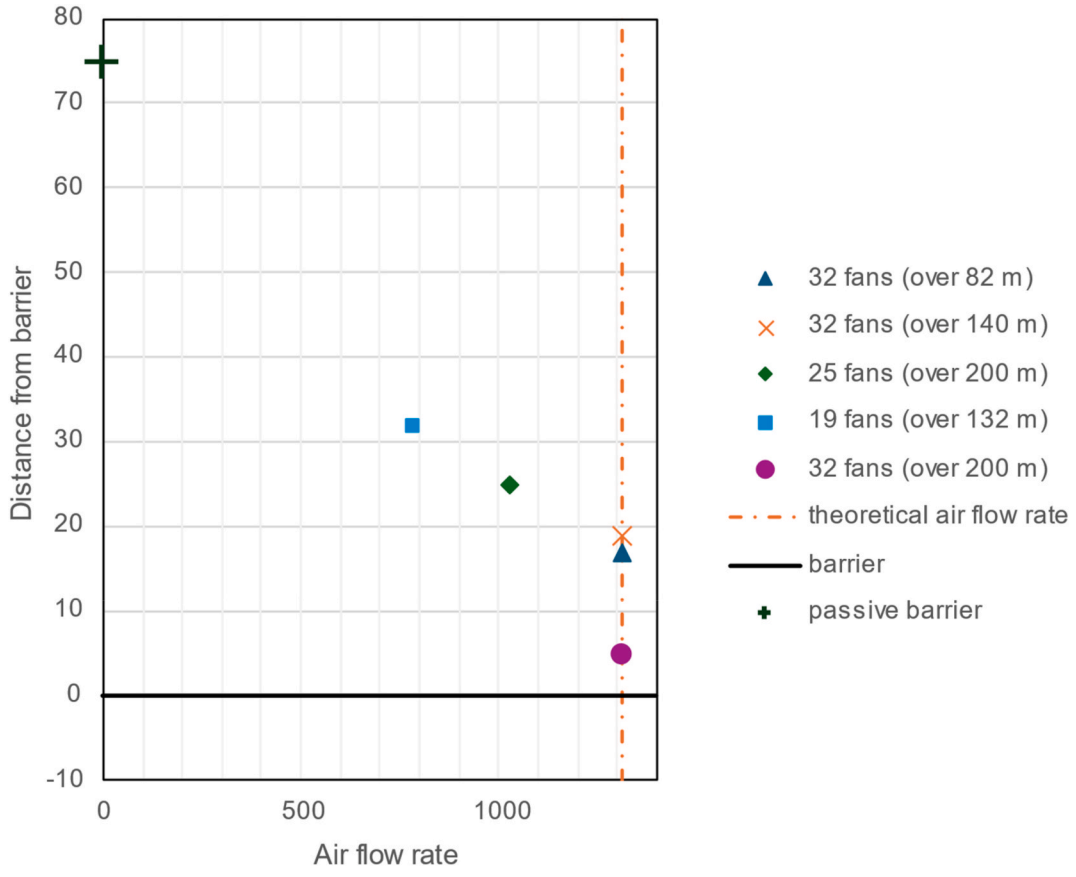

Fig. 12. Cloud distance as function of air flow rate.

the length of the portion of the barrier where the fans were embedded.

3.2.5. *Active barrier with 19 fans*

The effect of reducing simultaneously the number of fans (and therefore the overall air flow rate forced into the cloud) and the length of the portion of the barrier in which the fans are embedded was investigated by simulating a configuration of 19 fans, which is 40 % fewer than the theoretical number, distributed along 132 m of the barrier. Fig. 11 shows the LFL footprint of the cloud compared to the one of the passive barrier case.

We can see that reducing the air flow rate entering the cloud allows the LFL cloud envelope to overcome the barrier not only laterally but

Table 6
Active barrier parameters computed using the proposed procedure for case study B.

H^*_{cloud}	8.5 m
W^*_{cloud}	180 m
C_{max}	15 %
Q_c	7650 m^3/s
C_c	10.6 %
α	2.41
Q_a	10,779 m^3/s

also where the fans are installed.

3.3. Discussion

Table 6 summarizes the input of the simulations in terms of number of fans, width of wall along which they are distributed, and volume flow rate of air obtained and shows that the presence of a barrier always reduce the downwind cloud extension, while the cloud width and height increase.

Fig. 12 shows the hazardous distance (that is, the distance where the cloud concentration reaches LFL) downwind the barrier (since the barrier location can be safely reached by a flammable cloud) for the various configurations investigated. We can see that among the three configurations with the theoretical air flow rate (i.e., with 32 fans), the one with the fan placed over 200 m represent the best solution since the flammable cloud only overcomes the barrier by about 5 m. The remaining two configurations allow the cloud to overcome the barrier by about 17 m (since the cloud is wider than the portion of the barrier where the fans are installed, as previously seen). The configuration with 25 fans is a reasonable solution since it can reduce the cloud distance to about 25 m from the barrier with 22 % less air flow rate than the theoretical one. The configuration with 19 fans should also be taken in consideration since, with an air intake reduction of 40 % than the theoretical one, it can reduce the LFL cloud length to about 32 m from the barrier. In conclusion, while the passive barrier can reduce the flammable cloud distance from the pool by about 57 %, the implementation of an active barrier with fans is always able to further reduce the total flammable cloud length in a time of the order of 30 min.

To validate the proposed methodology, it was decided to further apply the active barrier design procedure to a second case involving a different release scenario, as discussed in the following.

4. Case study B

The second case study investigated involves a major accidental scenario. In this case study the leak is from a full-bore rupture of the same pipeline as in case A resulting in a boiling pool with constant diameter of 20 m and variable evaporation rate as shown in Fig. 13. For this case, the source term as well as the simulation data for open field case and passive

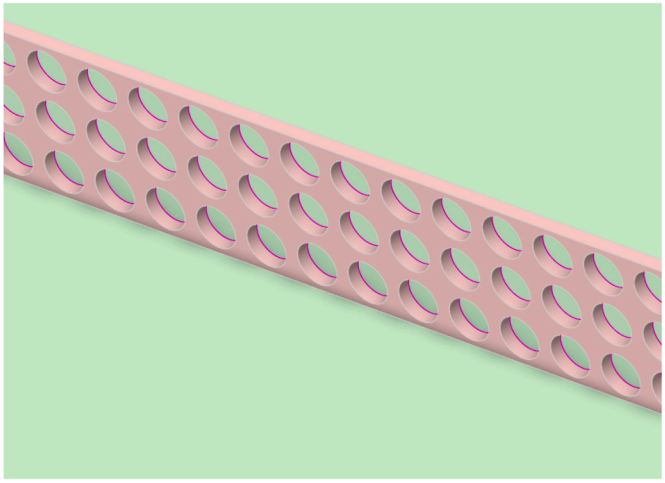

Fig. 14. Partial view of the fans embedded in the barrier.

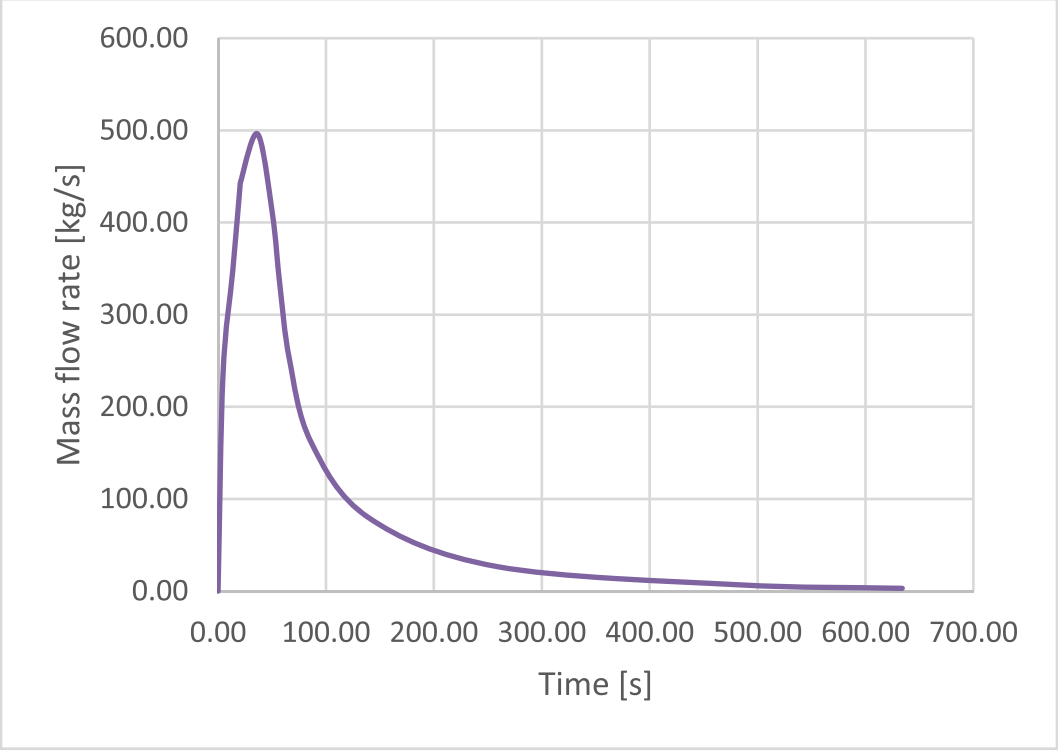

Fig. 13. Pool evaporation rate for case study B (Marsegan et al., 2016).

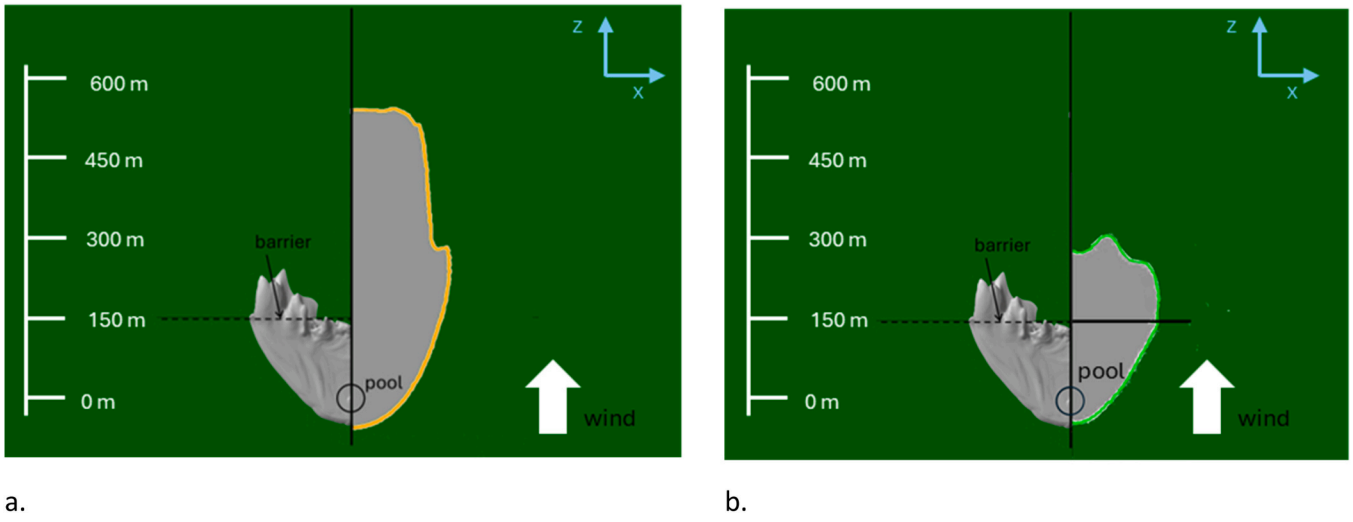

Fig. 15. a. LFL cloud envelope with the active barrier (left) and in open field conditions (right) for case study B (Busini and Rota, 2014; Marsegan et al., 2016); b. LFL cloud envelope with the active barrier (left) and in in presence of a 6 m high passive barrier (right) for case study B (Busini and Rota, 2014).

Table 7
Input of the simulations in terms of number of fans, power demand, width of wall along which they are distributed and volume flow rate of air obtained and output in terms of percentage difference of the cloud dimension at the LFL concentration with respect to the open field scenario for the various barrier configurations.

	Number of fans	Power demand [MW]	Barrier width [m]	Barrier width with fans embedded [m]	Qa [m3/s]	Length change [%]	Width change [%]	Height change [%]
Passive barrier[a]	0	0	450	–	0	−44	−15	n.a.
Active barrier	262	14	450	270	10,779	−61	0	n.a.

[a] Data from (Busini and Rota, 2014).

barrier case are taken from the work of (Marsegan et al., 2016).

Following the same procedure reported in section 2.1, the geometry and mesh were created and then loaded in the solver software.

This accidental scenario has been already investigated in the literature (Marsegan et al., 2016); from such results the parameters reported in Table 6 can be extrapolated. Using eq. (4), the theoretical air flow rate required to dilute the cloud can be calculated, resulting in an air injection rate of 10,779 m^3/s through the fans.

262 fans with the same size as in case A are required to face this scenario. They were located on three levels of the barrier as shown in Fig. 14, spanning on 270 m of the barrier (even though the W^*_{cld} parameter is 180 m, it is impossible to place 262 fans on such a short displacement, so it was decided to place them as close as possible). As for the case study A, the simulation began with only wind inlet, to gain stability and develop the overall wind profile along the domain; then, the pool mass flow inlet starts and, at the same time, the fans boundary conditions are activated, with the fan air flow direction opposite to the LNG cloud direction (that is, the wind direction).

The results reported in Fig. 15 show that the active barrier significantly reduces the downwind hazardous distance from the pool, which decrease from 600 m to 235 m, corresponding to a 61 % reduction with respect to the scenario without any barrier, and to 317 in case of the presence of a 6 m high wall; see also Table 7 for a resume of input and output of this simulation. While the active barrier is insufficient to contain the cloud at its location, it is important to note that the analysed case represents a catastrophic event with a statistically low probability of occurrence. According to (Casal, 2008) the frequency of a full-bore rupture in pipelines with diameters exceeding 150 mm is approximately 10^{-7} events per year. Therefore, it is evident that physical barriers, whether active or passive, should be considered as a last resort safety measure to mitigate the consequences of such highly improbable events. For the sake of comparison, a wall 6 m high not activated would reduce the LFL distance by 44 % (Busini and Rota, 2014), while to stop the cloud at the barrier in the same scenario, at least a 12 m high wall would be necessary (Marsegan et al., 2016). To implement an active air barrier, a 6-m-high inclined wall would be required, along with an airflow of approximately 1000 Nm^3/s sustained for around 300 s. This setup would demand the storage of roughly 3×10^5 Nm^3 of compressed air, ready for immediate deployment in case of an emergency. Using standard commercial tanks with a volume of 2.5 m^3, pressurized to 400 bar and standing 12 m tall, about 300 cylinders would be needed. These could be arranged in a cubic structure measuring $8 \times 8 \times 12$ m^3 (Marsegan et al., 2016).

The Supplementary Material includes a time-lapse image (Fig. S5) and a video showing the evolution of the cloud contour at the LFL concentration threshold over time. This visualization provides valuable insights from an emergency-response planning perspective, as it illustrates how the hazardous area develops and changes during the event. In particular, it is interesting to note that the fans are able to reduce the dimension of the LFL cloud inside the boundary of the plant in less than 4 min.

The practical feasibility of deploying 262 fans with a total power demand of 14 MW in Case B largely depends on the specific characteristics and infrastructure of the facility. While such a system could be technically implemented, it would require a substantial and rapid power supply, but the peak demand would occur only for a few minutes during an emergency (i.e., 5 min for the case here simulated). This raises concerns about power availability, system reliability, and maintenance. In comparison, alternative mitigation strategies such as water curtains may offer a more manageable and cost-effective solution. Water curtains can be activated quickly, require less energy, and are generally easier to integrate into existing safety systems. However, their effectiveness in controlling such a large vapor cloud dispersion may be lower than that

of high-capacity ventilation systems. Overall, while fan-based mitigation offers strong performance, its feasibility and cost-effectiveness must be carefully evaluated against simpler, more scalable alternatives. Notably, simulations show that the forced air entrainment into the cloud achieved by activating the fans (and anyway an active mitigation barrier) has a positive effect on reducing the damage distance, further supporting the potential benefit of this mitigation approach, despite its practical challenges in the case of catastrophic releases, which are, nonetheless, very unlikely.

5. Conclusions

In this study, two accidental scenarios involving an LNG pipeline rupture were analysed to assess the effectiveness of an active barrier in diluting an LNG cloud, which is representative of a dense gas cloud. The barrier, consisting of axial fans embedded in a wall, draws air upwind through the cloud, thereby enhancing dilution. In both scenarios, the barrier achieved a significant reduction in the cloud maximum downwind extension, which demonstrates the device effectiveness; a drawback is the power demand in case of catastrophic, but unlike, releases as discussed in the previous paragraph. In terms of practical safety outcomes, considering the flash fire as a plausible scenario in the event of a flammable vapor cloud dispersion, the presence of a barrier that prevents the lower flammable limit (LFL) from extending beyond the facility's boundaries can significantly impact societal risk. In particular, the high-fatality tail of the FN curve disappears, as all consequences remain confined within the site. Furthermore, individual risk levels outside the plant are effectively reduced to zero. However, a residual risk persists within the facility, emphasizing the importance of internal safety measures and emergency response planning to protect on-site personnel.

The simulations were performed in a 5D class as a representative scenario. To know exactly the influence of the atmospheric conditions *ad hoc* simulations would be necessary.

Finally, it should be noted that, in this work, the presented methodology was applied to LNG, as representative of dense gas clouds, and to the LFL as the threshold for flammable vapor dispersion distances, but the same methodology can be applied to the 50 % of the LFL threshold, as frequently done in industrial hazard study, or other concentration more significative for other gasses (e.g., threshold limits for toxic materials).

CRediT authorship contribution statement

Alessandro Pinciroli: Writing – original draft, Visualization, Software, Investigation, Formal analysis. **Renato Rota:** Writing – review & editing, Methodology, Conceptualization. **Valentina Busini:** Writing – review & editing, Supervision, Methodology, Data curation, Conceptualization.

Declaration of Competing Interest

The authors declare that they have no known competing financial interests or personal relationships that could have appeared to influence the work reported in this paper.

Acknowledgments

The authors gratefully acknowledge the contribution of Fabiana D'Onofrio, who conducted the preliminary version of this study.

Appendix A. Supplementary data

Supplementary data to this article can be found online at https://doi.org/10.1016/j.jlp.2025.105822.

Data availability

Data will be made available on request.

References

ANSYS Inc, 2023a. ANSYS Discovery Spaceclaim 23 Manual.
ANSYS Inc, 2023b. ANSYS Fluent 23 User's Guide.
Ayorinde, O.B., Daudu, C.D., Okoli, C.E., Adefemi, A., Adekoya, O.O., Ibeh, C.V., 2024. Reviewing the impact of LNG technology advancements on global energy markets. World J. Adv. Res. Rev. 21, 335–345. https://doi.org/10.30574/wjarr.2024.21.2.0462.
Baalisampang, T., Abbassi, R., Garaniya, V., Khan, F., Dadashzadeh, M., 2019. Accidental release of liquefied natural gas in a processing facility: effect of equipment congestion level on dispersion behaviour of the flammable vapour. J. Loss Prev. Process. Ind. 61, 237–248. https://doi.org/10.1016/j.jlp.2019.07.001.
Bellegoni, M., Ovidi, F., Landucci, G., Tognotti, L., Galletti, C., 2021. CFD analysis of the influence of a perimeter wall on the natural gas dispersion from an LNG pool. Process Saf. Environ. Prot. 148, 751–764. https://doi.org/10.1016/j.psep.2021.01.048.
Bellegoni, M., Ovidi, F., Tempesti, L., Mariotti, A., Tognotti, L., Landucci, G., Galletti, C., 2022. Optimization of gas detectors placement in complex industrial layouts based on CFD simulations. J. Loss Prev. Process. Ind. 80, 104859. https://doi.org/10.1016/j.jlp.2022.104859.
Brown, T.C., Cederwall, R.T., Chan, S.T., Ermak, D.L., Koopman, R.P., Lamson, K.C., McClure, J.W., Morris, L.K., 1990. Falcon Series Data Report: 1987 LNG Vapor Barrier Verification Field Trials (No. UCRL-CR-104316; GRI-89/0138). Lawrence Livermore National Lab. (LLNL), Livermore, CA (United States). https://doi.org/10.2172/6633087.
Buchlin, J.-M., 2017. Mitigation of industrial hazards by water spray curtains. J. Loss Prev. Process. Ind. 50, 91–100. https://doi.org/10.1016/j.jlp.2017.08.007.
Busini, V., Rota, R., 2014. Influence of the shape of mitigation barriers on heavy gas dispersion. J. Loss Prev. Process. Ind. 29, 13–21. https://doi.org/10.1016/j.jlp.2014.01.001.
Busini, V., Lino, M., Rota, R., 2012. Influence of large obstacles and mitigation barriers on heavy gas cloud dispersion: a liquefied natural gas case-study. Ind. Eng. Chem. Res. 51, 7643–7650. https://doi.org/10.1021/ie201591b.
Casal, J., 2008. Evaluation of the effects and consequences of major accidents in industrial plants. Industrial Safety Series, first ed. Elsevier, Amsterdam ; Boston.
Crowl, D.A., Louvar, J.F., 2019. Chemical process safety: fundamentals with applications. International Series in the Physical and Chemical Engineering Sciences, fourth ed. Pearson, Boston.
Daudu, C.D., Adefemi, A., Adekoya, O.O., Okoli, C.E., Ayorinde, O.B., Daraojimba, A.I., 2024. LNG and climate change: evaluating its carbon footprint in comparison to other fossil fuels. Eng. Sci. Technol. J. 5, 412–426. https://doi.org/10.51594/estj.v5i2.803.
Derudi, M., Bovolenta, D., Busini, V., Rota, R., 2014. Heavy gas dispersion in presence of large obstacles: selection of modeling tools. Ind. Eng. Chem. Res. 53, 9303–9310. https://doi.org/10.1021/ie4034895.
Diaz-Ovalle, C., Vazquez-Roman, R., Lesso-Arroyo, R., Mannan, M.S., 2012. A simplified steady-state model for air, water and steam curtains. J. Loss Prev. Process. Ind. 25, 974–981. https://doi.org/10.1016/j.jlp.2012.05.011.
DYNAIR, 2025. Ducted axial fan. Available at: https://www.dynair.it/en/products/cc/. accessed 7.21.25.
Eberwein, R., Rogge, A., Behrendt, F., Knaust, C., 2020. Dispersion modeling of LNG-vapor on land – a CFD-model evaluation study. J. Loss Prev. Process. Ind. 65, 104116. https://doi.org/10.1016/j.jlp.2020.104116.
Ennis, A., 2006. Development of source terms for gas dispersion and vapour cloud explosion modelling. Presented at the Institution of Chemical Engineers Symposium Series, pp. 108–121.
Fthenakis, V.M., Blewitt, D.N., 1993. Mitigation of hydrofluoric acid releases: simulation of the performance of water spraying systems. J. Loss Prev. Process. Ind. 6, 209–218. https://doi.org/10.1016/0950-4230(93)80002-4.
Gavelli, F., Bullister, E., Kytomaa, H., 2008. Application of CFD (fluent) to LNG spills into geometrically complex environments. In: J. Hazard. Mater., Papers Presented at the 2006 Annual Symposium of the Mary Kay O'Connor Process Safety Center, 159, pp. 158–168. https://doi.org/10.1016/j.jhazmat.2008.02.037.
Kim, B.K., Ng, D., Mentzer, R.A., Mannan, M.S., 2012. Modeling of water-spray application in the forced dispersion of LNG vapor cloud using a combined eulerian–lagrangian approach. Ind. Eng. Chem. Res. 51, 13803–13814. https://doi.org/10.1021/ie3003864.
Kim, B.K., Mentzer, R.A., Mannan, M.S., 2014. Numerical study on physical mechanisms of forced dispersion for an effective LNG spill mitigation. Ind. Eng. Chem. Res. 53, 9488–9498. https://doi.org/10.1021/ie400738p.
Koopman, R.P., Ermak, D.L., 2007. Lessons learned from LNG safety research. J. Hazard. Mater., LNG Special Issue - Dedicated to Risk Assessment and Consequence Analysis for Liquefied Natural Gas Spills 140, 412–428. https://doi.org/10.1016/j.jhazmat.2006.10.042.
Koopman, R.P., Ermak, D.L., Chan, S.T., 1989. A review of recent field tests and mathematical modelling of atmospheric dispersion of large spills of denser-than-air gases. Atmospheric Environ. 1967, International Conference on Tropical Micrometeorology and Air Pollution 23, 731–745. https://doi.org/10.1016/0004-6981(89)90475-7.

Lim, W., Choi, K., Moon, I., 2013. Current status and perspectives of liquefied natural gas (LNG) plant design. Ind. Eng. Chem. Res. 52, 3065–3088. https://doi.org/10.1021/ie302877g.

Lim, H., Um, K., Jung, S., 2017. A study on effective mitigation system for accidental toxic gas releases. J. Loss Prev. Process. Ind. 49, 636–644. https://doi.org/10.1016/j.jlp.2017.05.017.

Lyu, B., Lee, K., Kim, T., Cho, H., Moon, I., 2018. Damage reduction strategies against chemical accidents by using a mitigation barrier in Korean chemical risk management. Saf. Sci. 110, 29–36. https://doi.org/10.1016/j.ssci.2018.07.026.

Marsegan, C., Busini, V., Rota, R., 2016. Influence of active mitigation barriers on LNG dispersion. J. Loss Prev. Process. Ind. 44, 380–389. https://doi.org/10.1016/j.jlp.2016.10.010.

Min, D.S., Choi, S., Oh, E., Lee, J., Lee, C.-G., Choi, K., Jung, S., 2020. Numerical modelling for effect of water curtain in mitigating toxic gas release. J. Loss Prev. Process. Ind. 63, 103972. https://doi.org/10.1016/j.jlp.2019.103972.

Naveiro, M., Romero Gómez, M., Baaliña Insua, Á., Folgueras, M.B., 2021. Energy, exergy and economic analysis of offshore regasification systems. Int. J. Energy Res. 45, 20835–20866. https://doi.org/10.1002/er.7141.

Nerheim, A.R., Æsøy, V., Holmeset, F.T., 2021. Hydrogen as a maritime fuel–can experiences with LNG be transferred to hydrogen systems? J. Mar. Sci. Eng. 9, 743. https://doi.org/10.3390/jmse9070743.

Olewski, T., Nayak, S., Basha, O., Waldram, S., Véchot, L., 2011. Medium scale LNG-related experiments and CFD simulation of water curtain. In: J. Loss Prev. Process Ind., Papers Presented at the 2010 International Symposium of the Mary Kay O'Connor Process Safety Center, 24, pp. 798–804. https://doi.org/10.1016/j.jlp.2011.06.005.

PHAST, 2024. 9.0 Technical Reference Manual.

Pinciroli, A., Busini, V., Rota, R., 2024. Lng risk mitigation: a comparison between active and passive barriers. Chem. Eng. Trans. 111, 247–252. https://doi.org/10.3303/CET24111042.

Qi, M., Yue, T., Hua, M., Pan, X., Jiang, J., 2016. Experimental research on water curtain diluting heavy gas dispersion in limited space with no ventilation. J. Loss Prev. Process. Ind. 43, 471–478. https://doi.org/10.1016/j.jlp.2016.07.012.

Rana, M.A., Mannan, M.S., 2010. Forced dispersion of LNG vapor with water curtain. In: J. Loss Prev. Process Ind., Papers Presented at the 2009 International Symposium of the Mary Kay O'Connor Process Safety Center, 23, pp. 768–772. https://doi.org/10.1016/j.jlp.2010.08.008.

Rana, M.A., Guo, Y., Mannan, M.S., 2010. Use of water spray curtain to disperse LNG vapor clouds. J. Loss Prev. Process. Ind. 23, 77–88. https://doi.org/10.1016/j.jlp.2009.06.003.

Seshu, Dharmavaram, Dharmavaram, S., Steven, R. Hanna, Hanna, S.R., Olav, R. Hansen, Hansen, O.R., 2005. Consequence analysis—Using a CFD model for industrial sites. Process Saf. Prog. 24, 316–327. https://doi.org/10.1002/prs.10068.

Shingan, B., Banerjee, N., Kumawat, M., Mitra, P., Parthasarthy, V., Singh, V., 2024. Liquefied natural gas value chain: a comprehensive review and analysis. Chem. Eng. Technol. 47, 430–447. https://doi.org/10.1002/ceat.202300304.

Sun, B., Guo, K., Pareek, V.K., 2015. Dynamic simulation of hazard analysis of radiations from LNG pool fire. J. Loss Prev. Process. Ind. 35, 200–210. https://doi.org/10.1016/j.jlp.2015.04.010.

Tauseef, S.M., Tauseef, S.M., Rashtchian, Davood, Rashtchian, D., Abbasi, S.A., Abbasi, S.A., 2011. CFD-based simulation of dense gas dispersion in presence of obstacles. J. Loss Prev. Process. Ind. 24, 371–376. https://doi.org/10.1016/j.jlp.2011.01.014.

Uijt de Haag, P.A.M., Ale, B.J.M., Post, J.G., 2001. The 'Purple Book': guideline for quantitative risk assessment in the Netherlands. In: Pasman, H.J., Fredholm, O., Jacobsson, A. (Eds.), Loss Prevention and Safety Promotion in the Process Industries. Elsevier Science B.V., Amsterdam, pp. 1429–1438. https://doi.org/10.1016/B978-044450699-3/50053-7.

Wingstedt, E.M.M., Vartdal, M., Pettersson Reif, B.A., 2017. Large-eddy simulations of dense-gas dispersion within a high-Reynolds number turbulent boundary layer. Phys. Fluids 29, 095103. https://doi.org/10.1063/1.4999466.

Yun, G., Ng, D., Mannan, M.S., 2011. Key observations of liquefied natural gas vapor dispersion field test with expansion foam application. Ind. Eng. Chem. Res. 50, 1504–1514. https://doi.org/10.1021/ie100822h.